

Weak Adversarial Networks for High-dimensional Partial Differential Equations

Yaohua Zang ^{*} Gang Bao [†] Xiaojing Ye [‡] Haomin Zhou [§]

Abstract

Solving general high-dimensional partial differential equations (PDE) is a long-standing challenge in numerical mathematics. In this paper, we propose a transformative approach to solve high-dimensional linear and nonlinear PDEs defined on arbitrary domains by leveraging their weak formulations. We convert the problem of finding the weak solution of PDEs into an operator norm minimization problem induced from the weak formulation. The weak solution and the test function in the weak formulation are then parameterized as the primal and adversarial networks respectively, which are alternately updated to approximate the optimal network parameter setting. Our approach, termed as the weak adversarial network (WAN), is fast, stable, and completely mesh-free, which is particularly suitable for high-dimensional PDEs defined on irregular domains where the classical numerical methods based on finite differences and finite elements suffer the issues of slow computation, instability and the curse of dimensionality. We apply our method to a variety of test problems with high-dimensional PDEs to demonstrate its promising performance.

Keywords. High Dimensional PDE, Deep Neural Network, Adversarial Network, Weak Solution

1 Introduction

Solving general high-dimensional partial differential equations (PDE) has been a long-standing challenge in numerical analysis and computation [1, 2, 3, 4, 5, 6, 7, 8, 9, 10, 11, 12, 11]. A PDE defined on $\Omega \subset \mathbb{R}^d$ in a finite time horizon $[0, T]$ can be written in the following general form:

$$\begin{cases} \mathcal{A}[x, t; u(x, t)] = 0 & \text{in } \Omega \times [0, T] \\ \mathcal{B}[x, t; u(x, t)] = 0 & \text{on } \partial\Omega \times [0, T] \\ \mathcal{I}[x; u(x, 0)] = 0 & \text{in } \Omega \end{cases} \quad (1)$$

where $u : \Omega \times [0, T] \rightarrow \mathbb{R}$, $\mathcal{A}[\cdot]$ denotes the (possibly nonlinear) operator characterized by the PDE, $\mathcal{B}[\cdot] = 0$ stands for the boundary condition, and $\mathcal{I}[\cdot] = 0$ represents the initial value condition. For instance, in a general second-order parabolic PDE, $\mathcal{A}[\cdot] = 0$ corresponds to $u_t + \mathcal{L}(\nabla^2 u, \nabla u, u, x, t) = 0$ for some (possibly nonlinear) $\mathcal{L} : \mathbb{R}^{d \times d} \times \mathbb{R}^d \times \mathbb{R} \times \Omega \times [0, T] \rightarrow \mathbb{R}$ that couples u , ∇u , $\nabla^2 u$ and other given functions of x and t , where $\nabla u = (\partial_1 u, \dots, \partial_d u) \in \mathbb{R}^d$ is the (spatial) gradient of u , and $\nabla^2 u = [\partial_{ij}^2 u] \in \mathbb{R}^{d \times d}$ is the Hessian of u , with $\partial_i u = \partial u / \partial x_i$ and $\partial_{ij}^2 u = \partial^2 u / (\partial x_i \partial x_j)$ for short. Solving the initial boundary value condition problem (IBVP) (1) amounts to finding $u : \Omega \times [0, T] \rightarrow \mathbb{R}$ that satisfies the PDE $\mathcal{A}[\cdot] = 0$, the boundary value condition $\mathcal{B}[\cdot] = 0$, and the initial value $\mathcal{I}[\cdot] = 0$ in (1) simultaneously.

To instantiate the derivation of the proposed method, we will first focus on the second-order elliptic PDE with either Dirichlet's or Neumann's boundary conditions on *arbitrary domain* Ω . Specifically, a linear second-order elliptic PDE takes form

$$\begin{cases} -\sum_{i=1}^d \partial_i (\sum_{j=1}^d a_{ij} \partial_j u) + \sum_{i=1}^d b_i \partial_i u + cu - f = 0, & \text{in } \Omega \\ u(x) - g(x) = 0 \quad (\text{Dirichlet}) \quad \text{or} \quad (\partial u / \partial \vec{n})(x) - g(x) = 0 \quad (\text{Neumann}), & \text{on } \partial\Omega \end{cases} \quad (2)$$

^{*}School of Mathematical Sciences, Zhejiang University, Hangzhou, Zhejiang, China. Email: 11535015@zju.edu.cn.

[†]School of Mathematical Sciences, Zhejiang University, Hangzhou, Zhejiang, China. Email: baog@zju.edu.cn.

[‡]Department of Mathematics and Statistics, Georgia State University, Atlanta, Georgia 30303, USA. Email: xye@gsu.edu.

[§]School of Mathematics, Georgia Institute of Technology, Atlanta, Georgia 30332, USA. Email: hmzhou@math.gatech.edu.

where $a_{ij}, b_i, c : \Omega \rightarrow \mathbb{R}$ for $i, j \in [d] \triangleq \{1, \dots, d\}$, $f : \Omega \rightarrow \mathbb{R}$ and $g : \partial\Omega \rightarrow \mathbb{R}$ are all given, and $(\partial u / \partial \vec{n})(x)$ denotes the directional derivative of u along the outer normal direction \vec{n} at the boundary point $x \in \partial\Omega$. In addition, there exists a constant $\theta > 0$ such that $\xi^\top A(x) \xi \geq \theta |\xi|^2$ for any $\xi = (\xi_1, \dots, \xi_d) \in \mathbb{R}^d$ with $|\xi|^2 = \sum_{i=1}^d |\xi_i|^2$ and $x \in \Omega$ a.e., where $a_{ij} = a_{ji}$ for all $i, j \in [d]$ and $A(x) \triangleq [a_{ij}(x)] \in \mathbb{R}^{d \times d}$, i.e., $A(x)$ is symmetric positive definite with all eigenvalues no smaller than θ almost everywhere in Ω . We will also consider solving PDEs involving time, such as the linear second-order parabolic PDE (of finite time horizon):

$$\begin{cases} u_t - \sum_{i=1}^d \partial_i (\sum_{j=1}^d a_{ij} \partial_j u) + \sum_{i=1}^d b_i \partial_i u + cu - f = 0, & \text{in } \Omega \times [0, T] \\ u(x, t) - g(x, t) = 0 \quad (\text{Dirichlet}) \quad \text{or} \quad (\partial u / \partial \vec{n})(x, t) - g(x, t) = 0 \quad (\text{Neumann}), & \text{on } \partial\Omega \times [0, T] \\ u(x, 0) - h(x) = 0, & \text{on } \Omega \end{cases} \quad (3)$$

where $a_{ij}, b_i, c : \Omega \times [0, T] \rightarrow \mathbb{R}$ for $i, j \in [d]$ as before, $f : \Omega \times [0, T] \rightarrow \mathbb{R}$ and $g : \partial\Omega \times [0, T] \rightarrow \mathbb{R}$ and $h : \Omega \rightarrow \mathbb{R}$ are given. In either case, we will see that the method developed in this paper can be directly applied to *general high-dimensional linear and nonlinear PDEs*.

PDEs are prevalent and have extensive applications in science, engineering, economics, and finance [13, 14]. The standard approaches of numerical solutions to PDEs are finite difference and finite element methods (FEM) [15]. These methods discretize the time interval $[0, T]$ and the domain Ω using mesh grids or triangulations, create simple basis functions on the mesh, convert a continuous PDEs in (1) into its discrete counterpart, and finally solve the resulting system of basis coefficients to obtain numerical approximations of the true solution. Although these methods have been significantly advanced in the past decades and are able to handle rather complicated and highly oscillating problems, they suffer the so-called ‘‘curse of dimensionality’’ since the number of mesh points increases exponentially fast with respect to the problem dimension d and they quickly become computationally intractable in practice. As a consequence, these numerical methods are rarely useful for general high-dimensional PDEs, e.g. $d \geq 4$, especially when a sufficiently high-resolution solution is needed and/or the domain Ω is quite irregular, for which these methods can be slow and unstable.

In this paper, we provide a transformative approach to solve general high-dimensional PDEs defined on arbitrarily shaped domains. More specifically, we leverage the weak formulation of the PDEs, parametrize the weak solution and the test function as the primal and adversarial neural networks respectively, and train them in an unsupervised form where only the evaluations of these networks (and their gradients) on the sampled collocation points in the interior and boundary of the domain are needed. Our approach retains the continuum nature of PDEs for which partial derivatives can be carried out directly without any spatial discretization, and is fast and stable in solving general high-dimensional PDEs. Moreover, our method is completely mesh-free and can be applied to PDEs defined on arbitrarily shaped domains, without suffering the issue of the curse of dimensionality.

In the remainder of this paper, we first provide an overview of related work on solving PDEs using machine learning approaches in Section 2. In Section 3, we first consider static PDEs. We introduce the weak formulation of PDEs, reformulate the PDE as a saddle-point problem based on the operator norm induced from the weak formulation, and present our proposed algorithm with necessary training details. Then we extend the proposed method to solve PDEs involving time. In Section 4, we provide a number of numerical results to show that our method can solve high-dimensional PDEs efficiently and accurately. Section 5 concludes this paper.

2 Related Work

Deep learning techniques have emerged recently to solve PDEs. These methods can be roughly classified into two categories. In the first category, deep neural networks (DNN) are employed to assist the classical numerical methods. In [16], parallel neural networks are used to improve the efficiency of the finite difference method. In [17], neural network is used to accelerate the numerical methods for matrix algebra problems. Neural network is also applied to improve the accuracy of finite difference method in [18], which can be extended to solve two-dimensional PDEs [19]. In [20, 21], the solution of ordinary differential equations (ODE) is approximated by the combination of splines, where the combination parameters are determined by training a neural network with piecewise linear activation functions. A constrained integration method called

GINT is proposed to solving initial boundary value PDEs in [2], where neural networks are combined with the classical Galerkin method. In [22], convolutional neural networks (CNN) is used to solve the large linear system derived from the discretization of incompressible Euler equations. In [23], a neural network-based discretization scheme is developed for the nonlinear differential equation using regression analysis technique. Despite of the improvement over classical numerical methods, these methods still suffer the the exponentially increasing problem size and are not tractable for high-dimensional PDEs.

In the second category, the deep neural networks are employed to directly approximate the solution of PDE. In [3], the solution of the PDE is decomposed into two parts, where the first part is explicitly defined to satisfy the initial boundary conditions and the other part is a product of a mapping parametrized as a neural network and an explicitly defined function that vanishes on the boundary. Then the neural network is trained by minimizing the squared residuals over specified collocation points. In [24], an improvement of this method by parametrizing both parts using neural networks. The singular canonical correlation analysis (SVCCA) is introduced to further improve this method in [25]. In contrast to decomposing the solution into two parts, the idea of approximating the solution of PDEs by a single neural network is considered in [26], which is not capable of dealing with high-dimensional problems. In [4, 5], a class of physics informed (PI) deep learning models are developed to approximate the solution of PDEs by incorporating observed data points and initial boundary conditions into the loss function for training. A similar model is present in [27] for high dimensional parabolic PDEs and tested on free boundary problems. In [6, 7, 8, 9], a class of nonlinear PDEs represented as forward-backward stochastic differential equations are considered. In contrast, PDEs represented as variational problems are considered in [10, 11, 12]. In [10], a committer function is parameterized by a neural neural network whose weights are obtained by optimizing the variational formulation of the corresponding PDE. In [11], deep learning technique is employed to solve low-dimensional random PDEs based on both strong form and variational form. To the best of our knowledge, none of the existing methods consider the weak formulation of PDEs and model the test function as an adversarial network in combination as proposed in the present work.

3 Proposed Method

To demonstrate the main idea, we first focus on the boundary value problems (BVP) for static PDEs. We consider the weak formulation of the PDE, and interpret the weak solution finding problem as an operator norm minimization. The weak solution and the test function are both parametrized as deep neural networks, where the parameters are learned by an adversarial training governed by the weak formulation. Important implementation details are also provided. Finally, we extend the proposed method to the IBVP where the PDEs are time-dependent.

3.1 PDE and weak formulation

In general, a solution $u \in C^2(\Omega)$ of a BVP (2) requires sufficient regularity of the problem and may not exist in the classical sense. Instead, we consider the *weak formulation* of (2) by multiplying both sides by a test function $\varphi \in H_0^1(\Omega; \mathbb{R})$ and integrating by parts:

$$\begin{cases} \langle \mathcal{A}[u], \varphi \rangle \triangleq \int_{\Omega} \left(\sum_{j=1}^d \sum_{i=1}^d a_{ij} \partial_j u \partial_i \varphi + \sum_{i=1}^d b_i \varphi \partial_i u + cu\varphi - f\varphi \right) dx = 0 \\ \mathcal{B}[u] = 0, \quad \text{on } \partial\Omega \end{cases} \quad (4)$$

where $H_0^1(\Omega; \mathbb{R})$ denotes the Sobolev space, a Hilbert space of functions who themselves and their weak partial derivatives are L^2 integrable on Ω with vanishing trace on the boundary $\partial\Omega$. Note that the boundary terms of (4) after integration by parts disappears due to $\varphi = 0$ on $\partial\Omega$. If $u \in H^1(\Omega; \mathbb{R})$ with possibly nonzero trace satisfies (4) for all $\varphi \in H_0^1$, we say that u is a *weak solution* (or *general solution*) of (2). If certain conditions, such as elliptic regularity and those in the Sobolev's embedding theorem [28], hold, then the classical solution to (2) exists and coincides with the weak solution. In general, the weak solution to (2) may exist while a classical one may not. In this paper, we therefore seek for the weak solution characterized in (4) so that we can provide an answer to a BVP (2) to the best extent even if it does not admit a solution in the classical sense.

3.2 Induced operator norm minimization

The weak formulation (4) inspires a novel point of view of a weak solution u . Specifically, we can consider $\mathcal{A}[u] : H_0^1(\Omega) \rightarrow \mathbb{R}$ as a linear functional (operator) such that $\mathcal{A}[u](\varphi) \triangleq \langle \mathcal{A}[u], \varphi \rangle$ as defined in (4). Then the operator norm of $\mathcal{A}[u]$ induced from L^2 norm is defined by

$$\|\mathcal{A}[u]\|_{op} \triangleq \max\{\langle \mathcal{A}[u], \varphi \rangle / \|\varphi\|_2 \mid \varphi \in H_0^1, \varphi \neq 0\}, \quad (5)$$

where $\|\varphi\|_2 = (\int_{\Omega} |\varphi(x)|^2 dx)^{1/2}$. Therefore, u is a weak solution of (2) if and only if $\|\mathcal{A}[u]\|_{op} = 0$ and the boundary condition $\mathcal{B}[u] = 0$ is satisfied on $\partial\Omega$. As $\|\mathcal{A}[u]\|_{op} \geq 0$, we know that a weak solution u to (2) thus solves the following two equivalent problems in observation of (5):

$$\min_{u \in H^1} \|\mathcal{A}[u]\|_{op}^2 \iff \min_{u \in H^1} \max_{\varphi \in H_0^1} |\langle \mathcal{A}[u], \varphi \rangle|^2 / \|\varphi\|_2^2. \quad (6)$$

This result is summarized in the following theorem.

Theorem 1. *Suppose u^* satisfies the boundary condition $\mathcal{B}[u^*] = 0$, then u^* is a weak solution of the BVP (2) if and only if u^* solves the problems in (6) and $\|\mathcal{A}[u^*]\|_{op} = 0$.*

Proof. For any fixed $u \in H^1(\Omega)$, we can see that the maximum of $\langle \mathcal{A}[u], \varphi \rangle$ is achievable over $Y \triangleq \{\varphi \in H_0^1(\Omega) \mid \|\varphi\|_2 = 1\}$ since $\langle \mathcal{A}[u], \cdot \rangle$ is continuous and Y is closed in $H_0^1(\Omega)$. Denote $h(u)$ as the maximum of $\langle \mathcal{A}[u], \varphi \rangle$ over Y , then $h(u) = \|\mathcal{A}[u]\|_{op}$ in (5). On the other hand, the space of functions $u \in H^1(\Omega)$ satisfying the boundary condition $\mathcal{B}[u] = 0$, denoted by X , is also closed in $H^1(\Omega)$. Therefore, the minimum of $h(u)$ over X is also achievable. Hence the minimax problem (6) is well-defined.

Now we show that u^* is the solution of the minimax problem (6) if and only if it is the weak solution of the problem (2). Suppose u^* , satisfying the boundary condition $\mathcal{B}[u^*] = 0$, is the weak solution of the problem (2), namely u^* satisfies (4) for all $\varphi \in Y$, then $\langle \mathcal{A}[u^*], \varphi \rangle \equiv 0$ for all $\varphi \in Y$. Therefore, $\|\mathcal{A}[u^*]\|_{op} = 0$, and u^* is the solution of the minimax problem (6). On the other hand, suppose a weak solution \hat{u} of (2) exists. Assume that u^* is the minimizer of the problem (6), i.e., $u^* = \arg \min_{u \in X} h(u)$, but not a weak solution of the problem (2), then there exists $\varphi^* \in Y$ such that $\langle \mathcal{A}[u^*], \varphi^* \rangle > 0$. Therefore $h(u^*) = \max_{\varphi \in Y} |\langle \mathcal{A}[u^*], \varphi \rangle| > 0$. However, as we showed above, $h(\hat{u}) = 0$ since \hat{u} is a weak solution of (2), which contradicts to the assumption that u^* is the minimizer of $h(u)$ over X . Hence u^* must also be a weak solution of (2). \square

Theorem 1 implies that, to find the weak solution of (2), we can instead seek for the optimal solution u that minimizes (6).

3.3 Weak adversarial network for solving PDE

The formulation (6) inspires an adversarial approach to find the weak solution of (2). More specifically, we seek for the function $u_{\theta} : \mathbb{R}^d \rightarrow \mathbb{R}$, realized as a deep neural network with parameter θ to be learned, such that $\mathcal{A}[u_{\theta}]$ minimizes the operator norm (6). On the other hand, the test function φ , is a deep adversarial network with parameter η to be learned, challenges u_{θ} by maximizing $\langle \mathcal{A}[u_{\theta}], \varphi_{\eta} \rangle$ modulus its own norm $\|\varphi_{\eta}\|_2$ for every given u_{θ} in (6).

To train the deep neural network u_{θ} and the adversarial network φ_{η} such that they solve (6), we first need to formulate the objective functions of u_{θ} and φ_{η} . Since logarithm function is monotone and strictly increasing, we can for convenience reformulate (6) and obtain the objective of u_{θ} and φ_{η} in the interior of Ω as follows,

$$L_{\text{int}}(\theta, \eta) \triangleq \log |\langle \mathcal{A}[u_{\theta}], \varphi_{\eta} \rangle|^2 - \log \|\varphi_{\eta}\|_2^2. \quad (7)$$

In addition, the weak solution u_{θ} also need to satisfy the boundary condition $\mathcal{B}[u] = 0$ on $\partial\Omega$ as in (2). Let $\{x_b^{(j)}\}_{j=1}^{N_b}$ be a set of N_b collocation points on the boundary $\partial\Omega$, then the squared error of u_{θ} for Dirichlet boundary condition $u = g$ on $\partial\Omega$ is given by

$$L_{\text{bdry}}(\theta) \triangleq (1/N_b) \cdot \sum_{j=1}^{N_b} |u_{\theta}(x_b^{(j)}) - g(x_b^{(j)})|^2. \quad (8)$$

If the Neumann boundary condition in (2) is imposed in the BVP (2), then one can form the loss function $L_{\text{bdry}}(\theta) = (1/N_b) \cdot \sum_{j=1}^{N_b} |\sum_{i=1}^d n_i(x_b^{(j)}) \partial_i u_{\theta}(x_b^{(j)}) - g(x_b^{(j)})|^2$ instead, where $\vec{n}(x) = (n_1(x), \dots, n_d(x))$ is

the outer normal direction at $x \in \partial\Omega$. The total objective function is the weighted sum of the two objectives (7) and (8), for which we seek for a saddle point that solves the minimax problem:

$$\min_{\theta} \max_{\eta} L(\theta, \eta), \quad \text{where} \quad L(\theta, \eta) \triangleq \alpha L_{\text{int}}(\theta, \eta) + L_{\text{bdry}}(\theta), \quad (9)$$

where $\alpha > 0$ is user-chosen balancing parameter.

3.4 Training algorithm for the weak adversarial network

Given the objective function (9), the key ingredients in the network training are the gradients of $L(\theta, \eta)$ with respect to the network parameters θ and η . Then θ and η can be optimized by alternating gradient descent and ascend of $L(\theta, \eta)$ in (9) respectively.

To obtain the gradients of L_{int} in (9), we first denote the integrand of $\langle \mathcal{A}[u_{\theta}], \varphi_{\eta} \rangle$ in (4) as $I(x; \theta, \eta)$ for every given θ and η . For instance, for the second-order elliptic PDE (2), $I(x; \theta, \eta)$, $\nabla_{\theta} I(x; \theta, \eta)$, $\nabla_{\eta} I(x; \theta, \eta)$ are given below in light of the weak formulation (4):

$$\begin{aligned} I(x; \theta, \eta) &= \sum_{j=1}^d \sum_{i=1}^d a_{ij}(x) \partial_j u_{\theta}(x) \partial_i \varphi_{\eta}(x) + \sum_{i=1}^d b_i(x) \varphi_{\eta}(x) \partial_i u_{\theta}(x) \\ &\quad + c(x) u_{\theta}(x) \varphi_{\eta}(x) - f(x) \varphi_{\eta}(x) \\ \nabla_{\theta} I(x; \theta, \eta) &= \sum_{j=1}^d \sum_{i=1}^d a_{ij}(x) \partial_j \nabla_{\theta} u_{\theta}(x) \partial_i \varphi_{\eta}(x) + \sum_{i=1}^d b_i(x) \varphi_{\eta}(x) \partial_i \nabla_{\theta} u_{\theta}(x) \\ &\quad + c(x) \nabla_{\theta} u_{\theta}(x) \varphi_{\eta}(x) - f(x) \varphi_{\eta}(x) \\ \nabla_{\eta} I(x; \theta, \eta) &= \sum_{j=1}^d \sum_{i=1}^d a_{ij}(x) \partial_j u_{\theta}(x) \partial_i \nabla_{\eta} \varphi_{\eta}(x) + \sum_{i=1}^d b_i(x) \nabla_{\eta} \varphi_{\eta}(x) \partial_i u_{\theta}(x) \\ &\quad + c(x) u_{\theta}(x) \nabla_{\eta} \varphi_{\eta}(x) - f(x) \nabla_{\eta} \varphi_{\eta}(x) \end{aligned} \quad (10)$$

where $\nabla_{\theta} u_{\theta}$ and $\nabla_{\eta} \varphi_{\eta}$ are the standard gradients of the networks u_{θ} and φ_{η} with respect to their network parameters θ and η , respectively. Furthermore, due to the definition of L_{int} in (7) and the integrands in (10), we can obtain that $\nabla_{\theta} L_{\text{int}}(\theta, \eta) = 2(\int_{\Omega} I(x; \theta, \eta) dx)^{-1}(\int_{\Omega} \nabla_{\theta} I(x; \theta, \eta) dx)$. Then we randomly sample N_r collocation points $\{x_r^{(j)} \in \Omega \mid j \in [N_r]\}$ uniformly in the interior of the region Ω , and approximate the gradient $\nabla_{\theta} L_{\text{int}}(\theta, \eta) \approx (2/N_r) \cdot \sum_{j=1}^{N_r} (I(x_r^{(j)}; \theta, \eta))^{-1} (\nabla_{\theta} I(x_r^{(j)}; \theta, \eta))$. The gradients $\nabla_{\eta} L_{\text{int}}$, $\nabla_{\theta} L_{\text{bdry}}$ can be approximated similarly, and hence we omit the details here. With the gradients of $\nabla_{\theta} L$ and $\nabla_{\eta} L$, we can apply alternating updates to optimize the parameters θ and η . The resulting algorithm, termed as the weak adversarial network (WAN), is summarized in Algorithm 1.

3.5 Efficiency and stability improvements of WAN

During our experiments, we observed that several small modifications can further improve the efficiency and/or stability of Algorithm 1 in practice. One of these modifications is that, to enforce $\varphi_{\eta} = 0$ on Ω , we can factorize $\varphi_{\eta} = w \cdot v_{\eta}$, where w vanishes on $\partial\Omega$ and v_{η} is allowed to take any value on $\partial\Omega$. To obtain w for the domain Ω in a given BVP (2), we can set it to the signed distance function of Ω , i.e., $w(x) = \text{dist}(x, \partial\Omega) \triangleq \inf\{|x - y| : y \in \partial\Omega\}$ if $x \in \Omega$ and $-\text{dist}(x, \partial\Omega)$ if $x \notin \Omega$. This signed distance function can be obtained by the fast marching method. Alternatively, one can pretrain w as a neural network such that $w(x) > 0$ for $x \in \Omega$ and $w(x) = 0$ for $x \in \partial\Omega$. To this end, one can parametrize $w_{\xi} : \Omega \rightarrow \mathbb{R}$ as a neural network and optimize its parameter ξ by minimizing the loss function $\sum_{j=1}^{N_b} |w_{\xi}(x_b^{(j)})| - \varepsilon \sum_{j=1}^{N_r} \log w_{\xi}(x_r^{(j)})$. In either way, we precompute such w and fix it throughout Algorithm 1 WAN, then the updates of parameters are performed for u_{θ} and v_{η} only. In this case, $\varphi_{\eta} = w \cdot v_{\eta}$ always vanishes on $\partial\Omega$ so we do not need to worry about the boundary constraint of φ_{η} during the training.

In the training process for the neural network u_{θ} , we apply gradient descent directly to $|\langle \mathcal{A}[u_{\theta}], \varphi_{\eta} \rangle|^2$ without the logarithm which appears to improve efficiency. In addition, we find that the training process will be more stable by adding the following term to the loss function (9):

$$L_w(\theta) \triangleq |\langle \mathcal{A}[u_{\theta}], w \rangle|^2. \quad (11)$$

Therefore, the objective function for training u_{θ} becomes

$$L(\theta, \eta) \triangleq \alpha L_{\text{int}}(\theta, \eta) + \beta L_w(\theta) + L_{\text{bdry}}(\theta), \quad (12)$$

Algorithm 1 Weak Adversarial Network (WAN) for Solving High-dimensional static PDEs.

Input: N_r/N_b : number of region/boundary collocation points; K_u/K_φ : number of solution/adversarial network parameter updates per iteration.
Initialize: Network architectures $u_\theta, \varphi_\eta : \Omega \rightarrow \mathbb{R}$ and parameters θ, η .
while not converged **do**
 Sample collocation points $\{x_r^{(j)} \in \Omega : j \in [N_r]\}$ and $\{x_b^{(j)} \in \partial\Omega : j \in [N_b]\}$
 # update weak solution network parameter
 for $k = 1, \dots, K_u$ **do**
 Update $\theta \leftarrow \theta - \tau_\theta \nabla_\theta L$ where $\nabla_\theta L$ is approximated using $\{x_r^{(j)}\}$ and $\{x_b^{(j)}\}$ as in (10).
 end for
 # update test function network parameter
 for $k = 1, \dots, K_\varphi$ **do**
 Update $\eta \leftarrow \eta - \tau_\eta \nabla_\eta L$ where $\nabla_\eta L$ is approximated using $\{x_r^{(j)}\}$ as in (10).
 end for
end while
Output: Weak solution $u_\theta(\cdot)$ of (2).

where $\alpha, \beta > 0$ are user-chosen balancing parameters. The computer code that implements these modifications for all test problems in Section 4 will be released for public use upon acceptance of this paper.

3.6 Weak adversarial network for PDEs involving time

In this subsection, we consider extending the proposed weak adversarial network method to solve IBVPs with time-dependent PDEs. We provide two approaches for such case: one is to employ semi-discretization in time and iteratively solve $u(x, t_n)$ from a time-independent PDE for each t_n , where Algorithm 1 directly serves as a subroutine; the other one is to treat x and t jointly and consider the weak solution and test functions in the whole region $\Omega \times [0, T]$ without any discretization.

3.6.1 Semi-discretization in time

The weak adversarial network approach can be easily applied to time-dependent PDEs, such as the parabolic equation (3), by discretizing the time and solving an elliptical-type static PDE for each time point. To this end, we partition $[0, T]$ into N uniform segments using time points $0 = t_0 < t_1 < \dots < t_N = T$, and apply the Crank-Nicolson scheme [29] in classical finite difference method for (3) at each time t_n for $n = 0, \dots, N - 1$ to obtain

$$u(x, t_{n+1}) - u(x, t_n) = \frac{h}{2} \left(\mathcal{L}(x, t_{n+1}; u(x, t_{n+1})) + f(x, t_{n+1}) + \mathcal{L}(x, t_n; u(x, t_n)) + f(x, t_n) \right) \quad (13)$$

where $h = T/N$ is the time step size in discretization, $t_n = nh$, and

$$\mathcal{L}(x, t; u) \triangleq \sum_{i=1}^d \partial_i \left(\sum_{j=1}^d a_{ij}(x, t) \partial_j u(x, t) \right) - \sum_{i=1}^d b_i(x, t) \partial_i u(x, t) - c(x, t) u(x, t). \quad (14)$$

More precisely, we start with $u(x, t_0) = u(x, 0) = h(x)$, and solve for $u(x, t_1)$ from (13) for $n = 1$. Since (13) is an elliptical-type PDE in $u(x, t_1)$ with boundary value $u(x, t_1) = g(x, t_1)$ on $\partial\Omega$, we can apply Algorithm 1 directly and obtain $u(x, t_1)$ as the parametrized neural network $u_{\theta_1}(x)$ with parameter θ_1 output by Algorithm 1. Following this procedure, we can solve (13) for $u(x, t_n) = u_{\theta_n}(x)$ for $n = 2, 3, \dots, N$ in order. This process is summarized in Algorithm 2. Other types of time discretization can be employed and the IBVP can be solved with similar idea.

3.6.2 Solving PDE with space and time variables jointly

The proposed weak adversarial network approach can also be generalized to solve the IBVP (3) with space and time variables jointly. In this case, the *weak formulation* of (3) can be obtained by multiplying both

Algorithm 2 Solving parabolic PDE (3) with semi-discretization in time and Algorithm 1 as subroutine

Input: N_r, N_b, K_u, K_φ as in Algorithm 1. N : number of time points; $h = T/N$.
Initialize: Network architectures $u_\theta, \varphi_\eta : \Omega \rightarrow \mathbb{R}$ and parameters θ, η for each t_n . Set $u(x, t_0) = u(x, 0) = h(x)$.
for $n = 0, \dots, N - 1$ **do**
 Solve for $u(x, t_{n+1}) = u_{\theta_{n+1}}(x)$ from the elliptical equation (13) using Algorithm 1
end for
Output: Weak solution $u_\theta(\cdot, t_n)$ of (3) for $n = 1, \dots, N$.

Algorithm 3 Weak Adversarial Network (WAN) for Solving high-dimensional PDEs in whole space $\Omega \times [0, T]$

Input: $N_r/N_b/N_a$: number of region/boundary/initial collocation points; K_u/K_φ . $\Omega_T \triangleq \Omega \times [0, T]$.
Initialize: Network architectures $u_\theta, \varphi_\eta : \Omega_T \rightarrow \mathbb{R}$ and parameters θ, η .
while not converged **do**
 Sample points $\{(x_r^{(j)}, t_r^{(j)}) : j \in [N_r]\} \subset \Omega_T, \{(x_b^{(j)}, t_b^{(j)}) : j \in [N_b]\} \subset \partial\Omega \times [0, T], \{x_a^{(j)} : j \in [N_a]\} \subset \Omega$
 # update weak solution network parameter
 for $k = 1, \dots, K_u$ **do**
 Update $\theta \leftarrow \theta - \tau_\theta \nabla_\theta L$ where $\nabla_\theta L$ in (16) is approximated using $\{(x_r^{(j)}, t_r^{(j)})\}$ and $\{(x_b^{(j)}, t_b^{(j)})\}$ and $\{x_a^{(j)}\}$.
 end for
 # update test function network parameter
 for $k = 1, \dots, K_\varphi$ **do**
 Update $\eta \leftarrow \eta - \tau_\eta \nabla_\eta L$ where $\nabla_\eta L$ in (16) is approximated using $\{(x_r^{(j)}, t_r^{(j)})\}$.
 end for
end while
Output: Weak solution $u_\theta(x, t)$ in Ω_T .

sides of (3) by a test function $\varphi(\cdot, t) \in H_0^1(\Omega)$ a.e. in $[0, T]$ and integrating by parts:

$$0 = \langle \mathcal{A}[u], \varphi \rangle \triangleq \int_\Omega (u(x, T)\varphi(x, T) - h(x)\varphi(x, 0)) dx - \int_0^T \int_\Omega u \partial_t \varphi dx dt + \int_0^T \int_\Omega (\sum_{j=1}^d \sum_{i=1}^d a_{ij} \partial_j u \partial_i \varphi + \sum_{i=1}^d b_i \varphi \partial_i u + cu\varphi - f\varphi) dx dt \quad (15)$$

Following the same idea presented in Section 3.2–3.3, we parametrize the weak solution u and test function φ as deep neural networks $u_\theta, \varphi_\eta : \Omega \times [0, T] \rightarrow \mathbb{R}$ with parameters θ and η respectively. Then we form the objective function in the saddle-point problem of θ and η as

$$L(\theta, \eta) \triangleq \alpha L_{\text{int}}(\theta, \eta) + \gamma L_{\text{init}}(\theta) + L_{\text{bdry}}(\theta), \quad (16)$$

where $\alpha, \gamma > 0$ are user-chosen balancing parameters. In (16), the loss function L_{int} of the interior of $\Omega \times [0, T]$ has the same form as (7) but with $\langle \mathcal{A}[u_\theta], \varphi_\eta \rangle$ defined in (15) and $\|\varphi_\eta\|_2^2 \triangleq \int_0^T \int_\Omega |\varphi(x, t)|^2 dx dt$; L_{init} of the initial value condition in Ω and L_{bdry} of the boundary value condition on $\partial\Omega \times [0, T]$ are given by

$$L_{\text{init}}(\theta) \triangleq (1/N_a) \cdot \sum_{j=1}^{N_a} |u_\theta(x_a^{(j)}, 0) - h(x_a^{(j)})|^2 \quad (17)$$

$$L_{\text{bdry}}(\theta) \triangleq (1/N_b) \cdot \sum_{j=1}^{N_b} |u_\theta(x_b^{(j)}, t_b^{(j)}) - g(x_b^{(j)}, t_b^{(j)})|^2 \quad (18)$$

where $\{x_a^{(j)} : j \in [N_a]\} \subset \Omega$ are N_a collocation points for the initial condition and $\{(x_b^{(j)}, t_b^{(j)}) : j \in [N_b]\} \subset \partial\Omega \times [0, T]$ are N_b collocation points for the boundary condition.

Similar as in Section 3.5, we factorize $\varphi_\eta = w \cdot v_\eta$ where $w : \Omega_T \rightarrow \mathbb{R}$ is set to a function which vanishes on $\partial\Omega \times [0, T]$ in advance, and then we add the term $\beta L_w(\theta)$ which has the same form as (11) to (16). The training process is similar as above, which is summarized in Algorithm 3.

Table 1: List of model and algorithm parameters.

Notation	Stands for ...
d	Dimension of $\Omega \subset \mathbb{R}^d$
K_φ	Inner iteration to update test function φ_η
K_u	Inner iteration to update weak solution u_θ
τ_η	Learning rate for network parameter η of test function φ_η
τ_θ	Learning rate for network parameter θ of weak solution u_θ
N_r	Number of sampled collocation points in the region Ω
N_b	Number of sampled collocation points on the boundary $\partial\Omega$ or $\partial\Omega \times [0, T]$
N_a	Number of sampled collocation points in $\Omega = \Omega \times \{0\}$ at initial time
α	Weight parameter of $L_{\text{int}}(\theta, \eta)$ in the interior of Ω
β	Weight parameter of $L_w(\theta)$
γ	Weight parameter of $L_{\text{init}}(\theta)$ for the initial value condition

4 Experimental results

4.1 Experiment setup

In this section, we conduct a series of numerical experiments of the proposed algorithms (Algorithms 1–3) on BVP and IBVP with high-dimensional linear and *nonlinear* PDEs defined on regular and *irregular* domains. To quantitatively evaluate the accuracy of a solution u_θ , we compute the relative error $\|u_\theta - u^*\|_2 / \|u^*\|_2$, where u^* is the exact solution of the problem and u_θ is the result obtained by the our algorithm. In all experiments, we set both of the primal network (weak solution u_θ) and the adversarial network (test function φ_η) as fully-connected feedforward networks. The u_θ network has a total of 7 layers including the input and output layers, where each hidden layer contains 50 neurons. The activation functions is tanh for layers 1,2,4,6 and softplus for layers 3,5, and identity for the last layer. For the network φ_η , it consists of a total of 9 layers with each hidden layer containing 50 neurons. The activation functions is tanh for layers 1,2, softplus for layers 3,5,8, sinc for layers 2,5,7, and identity for the last layer. These two networks are trained by minimizing the loss function (9) or (16) by AdamGrad [30]. All model and algorithm parameters are summarized in Table 1 for quick reference. The values of these parameters are given in the description of each experiment below. The algorithm and numerical experiments are implemented in the TensorFlow [31] framework.

4.2 High-dimensional nonlinear elliptic PDEs with Dirichlet boundary condition

We first conduct a numerical test of Algorithm 1 on a *nonlinear* elliptic PDEs with Dirichlet boundary condition as follows,

$$\begin{cases} -\nabla \cdot (a(x)\nabla u) + \frac{1}{2}|\nabla u|^2 = f(x) & \text{in } \Omega \triangleq (-1, 1)^d, \\ u(x) = g(x) & \text{on } \partial\Omega \end{cases} \quad (19)$$

where $a(x) = 1 + |x|^2$ in Ω , $f(x) = 4\rho_1^2(1 + |x|^2) \sin \rho_0^2 - 4\rho_0^2 \cos(\rho_0^2) - (\pi + 1)(1 + |x|^2) \cos(\rho_0^2) + 2\rho_1^2 \cos^2(\rho_0^2)$ in Ω , and $g(x) = \sin(\frac{\pi}{2}x_1^2 + \frac{1}{2}x_2^2)$ on $\partial\Omega$, with $\rho_0^2 \triangleq \frac{\pi}{2}x_1^2 + \frac{1}{2}x_2^2$, $\rho_1^2 \triangleq \frac{\pi^2}{2}x_1^2 + \frac{1}{2}x_2^2$. The exact solution of (19) is $u^*(x) = \sin(\frac{\pi}{2}x_1^2 + \frac{1}{2}x_2^2)$ in Ω . We tested Algorithm 1 on the BVP (19) with problem dimensions $d = 2, 3, 4, 5$. For all dimensions, we set $K_\phi = 1$, $K_u = 2$, $\tau_\eta = 0.04$, $\tau_\theta = 0.018$, $N_r = 5 \times 10^4$, $\alpha = 0.001$ and $\beta = 0.1$. We set $N_b = 10^4, 3.84 \times 10^4, 10^6, 4 \times 10^6$ for $d = 2, 3, 4, 5$, respectively. Figure 1 shows the exact solution u^* and the approximation u_θ obtained by Algorithm 1 after 10,000 iterations. The pointwise absolute error $|u(x) - u^*(x)|$ in Ω for $d = 2, 3, 4, 5$ cases (we take slice $x_3 = \dots = x_d = 0$ for display when $d \geq 3$) is shown in Figure 2 (note the smaller scale bar compared to Figure 1). In Figure 3, we show the relative error $\|u_\theta - u^*\|_2 / \|u^*\|_2$ versus iteration number for $d = 2, 3, 4, 5$ cases, respectively. After 10,000 iterations, the final relative errors $\|u_\theta - u^*\|_2 / \|u^*\|_2$ achieve 2.53%, 0.72%, 1.43% and 1.35% for these cases, respectively. These plots show that Algorithm 1 can consistently generate accurate solutions of nonlinear

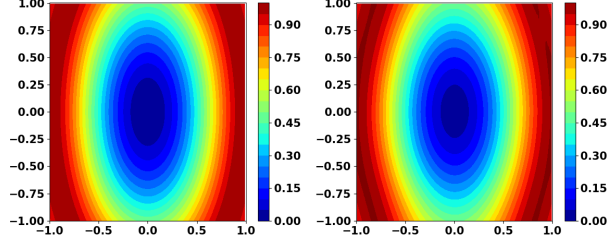


Figure 1: Exact solution u^* (left) and the approximation u_θ (right) obtained by Algorithm 1 for the BVP with nonlinear elliptic PDE (19) in $d = 2$ case.

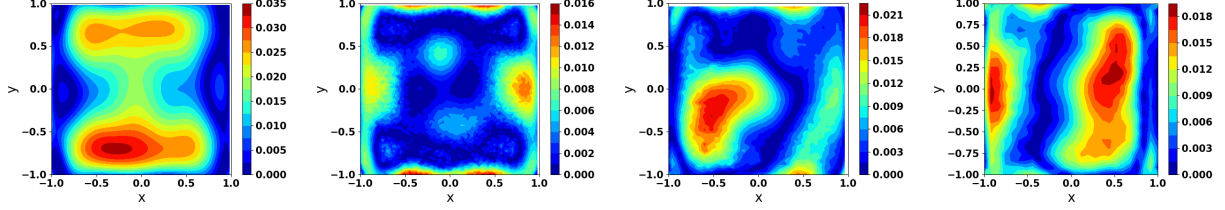


Figure 2: From left to right: pointwise absolute error $|u(x) - u^*(x)|$ obtained by Algorithm 1 on the nonlinear elliptical PDE (19) with $d = 2, 3, 4, 5$, respectively. For display purpose, the right three error images only show the slices of $x_3 = \dots = x_d = 0$ for $d \geq 3$ cases.

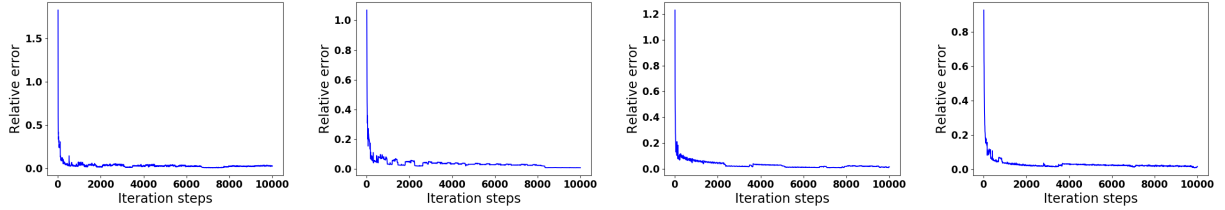


Figure 3: From left to right: relative errors versus iteration number of Algorithm 1 on the BVP with nonlinear elliptic PDE (19) for problem dimensions $d = 2, 3, 4, 5$, respectively.

PDEs in high dimensional case.

4.3 Poisson equation with Neumann boundary condition

We also consider solving a high-dimensional second order elliptical equation with *Neumann* boundary condition:

$$\begin{cases} -\Delta u + 2u = f & \text{in } \Omega \triangleq (0, 1)^d, \\ \frac{\partial u}{\partial \vec{n}} = g & \text{on } \partial\Omega \end{cases} \quad (20)$$

We set $f(x) = (\frac{\pi^2}{2} + 2) \sin(\frac{\pi}{2}x_1) \cos(\frac{\pi}{2}x_2)$ and

$$g(x) \triangleq \left[\frac{\pi}{2} \cos\left(\frac{\pi}{2}x_1\right) \cos\left(\frac{\pi}{2}x_2\right), -\frac{\pi}{2} \sin\left(\frac{\pi}{2}x_1\right) \sin\left(\frac{\pi}{2}x_2\right), 0, \dots, 0 \right] \cdot \vec{n} \quad \text{on } \partial\Omega$$

where \vec{n} is the outer normal vector on $\partial\Omega$. The exact solution of (20) is $u(x) = \sin(\frac{\pi}{2}x_1) \cos(\frac{\pi}{2}x_2)$ in Ω . In this experiment, we set $K_\varphi = 2$, $K_u = 4$ (5 for $d = 5$), $\tau_\eta = 0.05$, $\tau_\theta = 0.02$ (0.024 for $d = 5$), $N_r = 6 \times 10^3, 6 \times 10^4, 6 \times 10^4, 1.2 \times 10^5$, $N_b = 10^4, 3.84 \times 10^4, 10^6, 4 \times 10^6$, $\alpha = 0.02, 0.04, 0.1, 0.4$, and $\beta = 1$ for $d = 2, 3, 4, 5$ respectively. Figure 4 shows the exact solution u^* (left) and the solution u_θ by Algorithm 1 in $d = 2$ case. Figure 5 shows the point-wise absolute error $|u_\theta(x) - u^*(x)|$ and Figure 6 plots the progress of the relative error versus iteration number for $d = 2, 3, 4, 5$ cases, respectively. After 10,000 iterations, the final relative errors are 1.69%, 1.91%, 3.55%, 4.55% for $d = 2, 3, 4, 5$ cases, respectively. These results

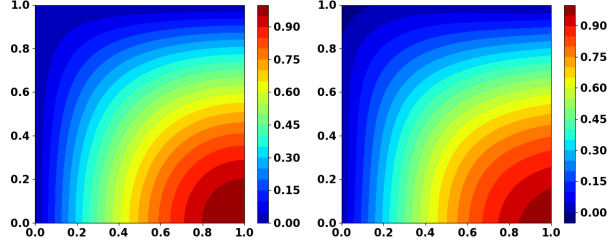


Figure 4: Exact solution u^* (left) and the approximation u_θ (right) obtained by Algorithm 1 for the BVP with Neumann boundary condition (20) in $d = 2$ case.

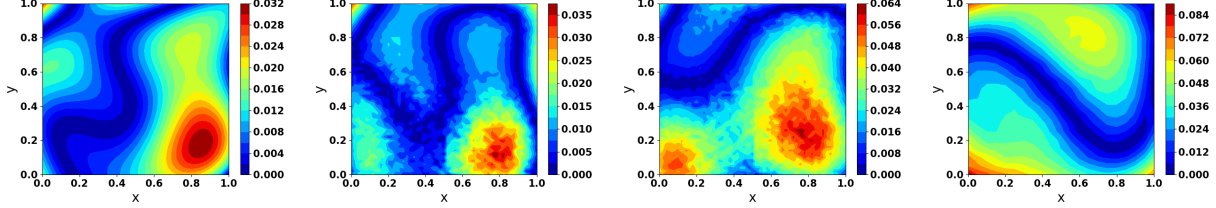


Figure 5: From left to right: pointwise absolute error $|u(x) - u^*(x)|$ obtained by Algorithm 1 after 10,000 iterations on the BVP with Neumann boundary condition (20) with $d = 2, 3, 4, 5$, respectively. For display purpose, the right three error images only show the slices of $x_3 = \dots = x_d = 0$ for $d \geq 3$.

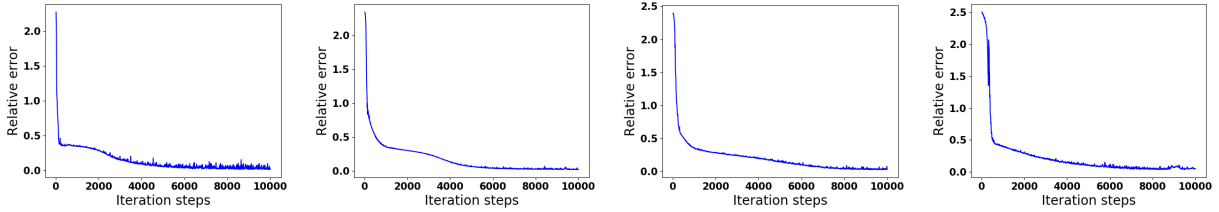


Figure 6: From left to right: relative errors versus iteration number of Algorithm 1 on the BVP with Neumann boundary condition (20) for problem dimensions $d = 2, 3, 4, 5$, respectively.

show that Algorithm 1 can consistently generate highly accurate solutions for various problem dimensions for BVP with Neumann boundary condition.

4.4 Poisson equation on irregular nonconvex domain

We further test Algorithm 1 on a BVP defined on an *irregular* nonconvex domain Ω . We again use anisotropic Poisson equation in the BVP specified below:

$$\begin{cases} -\nabla \cdot (a(x)\nabla u) = f(x) & \text{in } \Omega \triangleq (-1, 1)^d \setminus [0, 1)^d \\ u(x) = g(x) & \text{on } \partial\Omega \end{cases} \quad (21)$$

This problem is considered very challenging for the classical numerical methods, such as the finite difference method [32], which can be unstable for problems defined on nonconvex domains. In this experiment, we set $a(x) = 1 + |x|^2$ and $f(x) = \frac{\pi^2}{2} \cdot (1 + |x|^2) \sin(\tilde{x}_1) \cos(\tilde{x}_2) + \pi x_2 \sin(\tilde{x}_1) \sin(\tilde{x}_2) - \pi x_1 \cos(\tilde{x}_1) \cos(\tilde{x}_2)$ in Ω and $g(x) = \sin(\tilde{x}_1) \cos(\tilde{x}_2)$ on $\partial\Omega$, with $\tilde{x}_i \triangleq (\pi/2) \cdot x_i$ for $i = 1, 2$. The true solution is $u^* = \sin(\tilde{x}_1) \cos(\tilde{x}_2)$ in Ω . In this experiment, we set $K_\varphi = 2$, $K_u = 5$, $\tau_\eta = 0.05$, $\tau_\theta = 0.018$, $N_r = 10^4, 5 \times 10^4, 5 \times 10^4, 5 \times 10^4$, $N_b = 10^3, 7.5 \times 10^3, 10^4, 1.25 \times 10^4$, $\alpha = 0.1$, and $\beta = 1$ for $d = 2, 3, 4, 5$ respectively. We first test Algorithm 1 (21) with problem dimension $d = 2$. In this case Ω is an L-shaped domain in \mathbb{R}^2 as shown in Figure 7. The exact solution u^* and the approximation u_θ obtained by Algorithm 1 after 10,000 iterations are shown in the left and right panels of Figure 7 respectively. The relative error of u_θ is 4.8%. As we can see,

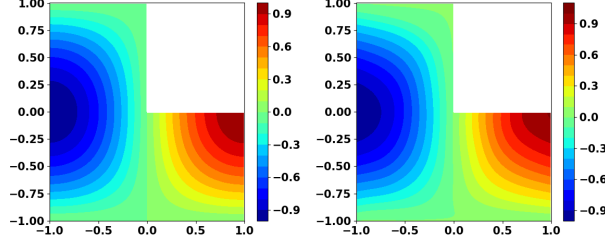


Figure 7: Exact solution u^* (left) and the approximation u_θ (right) obtained by Algorithm 1 for BVP (21) defined on the nonconvex L-shaped domain Ω for dimension $d = 2$.

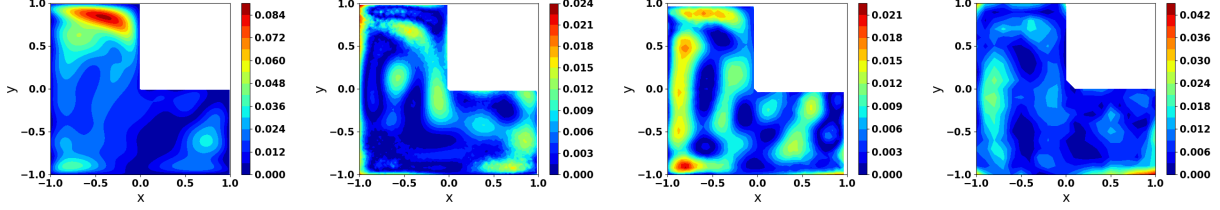


Figure 8: From left to right: pointwise absolute error $|u(x) - u^*(x)|$ obtained by Algorithm 1 on BVP (21) defined on nonconvex domain Ω with $d = 2, 3, 4, 5$, respectively. For display purpose, the right three error images show the slices of $x_3 = \dots = x_d = 0$ for $d \geq 3$ cases, respectively.

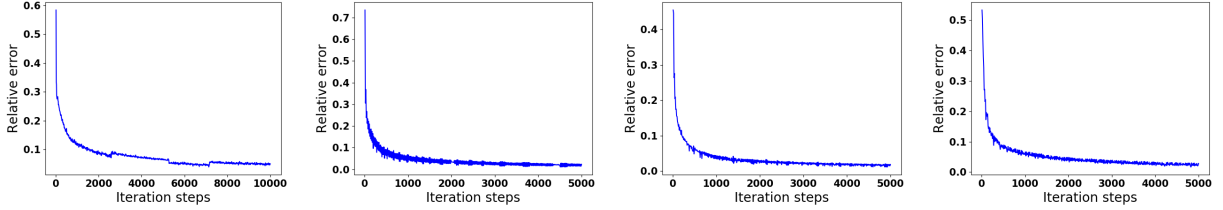


Figure 9: From left to right: relative errors versus iteration number of Algorithm 1 on the BVP (21) with nonconvex domain for problem dimensions $d = 2, 3, 4, 5$, respectively.

Algorithm 1 produces very promising approximation to the true solution u^* for this highly challenging BVP with nonconvex domain Ω .

We further conduct tests of Algorithm 1 on the BVP (21) with higher dimensions $d = 3, 4, 5$. Note that N_r remains the same, and N_b only increase moderately as the problem dimension d increases. The pointwise absolute error $|u(x) - u^*(x)|$ obtained by Algorithm 1 for BVP (21) with problem dimensions $d = 2, 3, 4, 5$ are shown in Figure 8. Note that the results for $d = 3, 4, 5$ are obtained with only 5,000 iterations (compared to 10,000 for $d = 2$). The progress of relative error versus iteration number for $d = 2, 3, 4, 5$ are shown in Figure 9, which demonstrates that Algorithm 1 can stably approximate the true solution even if the domain is irregular. The relative error of u_θ from u^* are 4.80%, 1.49%, 1.88% and 2.26% for problem dimension $d = 2, 3, 4, 5$, respectively.

4.5 High-dimensional partial differential equations involving time

In the last test, we consider solving the following *nonlinear* diffusion-reaction equation:

$$\begin{cases} u_t - \Delta u - u^2 = f(x, t), & \text{in } \Omega \times [0, T] \\ u(x, t) = g(x, t), & \text{on } \partial\Omega \times [0, T] \\ u(x, 0) = h(x), & \text{in } \Omega \end{cases} \quad (22)$$

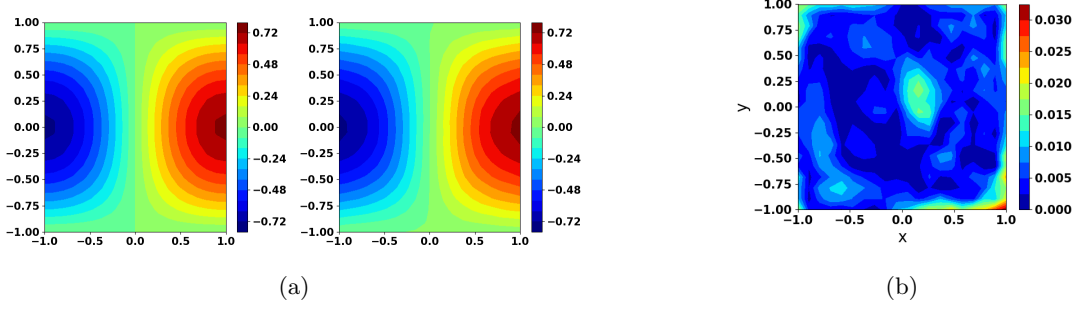


Figure 10: (a): Exact solution $u^*(x, T)$ (left) and the approximation $u_\theta(x, T)$ (right) obtained by Algorithm 2 at final time $T = 1$ for the IBVP (22) with problem dimension $d = 5$. (b): The corresponding point-wise absolute error $|u(x, T) - u^*(x, T)|$. All images only show the 2D slice of $x_3 = x_4 = 0$ for display purpose.

where $\Omega = (0, 1)^d$. We first give an example of solving the IBVP (22) in dimension $d = 5$ using Algorithm 2 which discretizes time and uses the Crank-Nicolson scheme (13). In this test, we set $f(x, t) = (\pi^2 - 2) \sin(\frac{\pi}{2}x_1) \cos(\frac{\pi}{2}x_2)e^{-t} - 4 \sin^2(\frac{\pi}{2}x_1) \cos(\frac{\pi}{2}x_2)e^{-2t}$ in $\Omega \times [0, T]$, $g(x, t) = 2 \sin(\frac{\pi}{2}x_1) \cos(\frac{\pi}{2}x_2)e^{-t}$ on $\partial\Omega \times [0, T]$ and $h(x) = 2 \sin(\frac{\pi}{2}x_1) \cos(\frac{\pi}{2}x_2)$ in Ω . In this case, the exact solution of the IBVP (22) is $u(x, t) = 2 \sin(\frac{\pi}{2}x_1) \cos(\frac{\pi}{2}x_2)e^{-t}$. We take $T = 1$ and discretize the time interval $[0, 1]$ into $N = 10$ equal segments, and then solve the IBVP using Algorithm 2. Figure 10(a) shows the exact solution u^* (left) and the solution u_θ (right) obtained by Algorithm 2 at final time T . Figure 10(b) shows the point-wise absolute error $|u_\theta(x, T) - u^*(x, T)|$. The absolute L^2 error and the relative error for this scheme are 1.003×10^{-2} and 2.8% respectively. The small error implies that the solution obtained by Algorithm 2 is a close approximation to the true solution u^* .

We also considered solving the diffusion-reaction equation (22) for space dimension $d = 1, 2, 3, 4$ using Algorithm 3 by dealing with (x, t) jointly without discretization. Unlike Algorithm 2 which solves for $u(x, t)$ for t at time grid points $\{t_n : n \in [N]\}$, Algorithm 3 provides a solution $u(x, t)$ that can be evaluated at *any* time in $[0, T]$. In this experiment, we set $f(x, t) = (\frac{\pi^2}{2} - 2) \sin(\frac{\pi}{2}x_1)e^{-t} - 4 \sin^2(\frac{\pi}{2}x_1)e^{-2t}$ in $\Omega \times [0, T]$, $g(x, t) = 2 \sin(\frac{\pi}{2}x_1)e^{-t}$ on $\partial\Omega \times [0, T]$, and $h(x) = 2 \sin(\frac{\pi}{2}x_1)$ in Ω . The exact solution is $u(x, t) = 2 \sin(\frac{\pi}{2}x_1)e^{-t}$ in $\Omega \times [0, T]$. We set $K_\varphi = 2, K_u = 5, \tau_\eta = 0.04, \tau_\theta = 0.02, \beta = 1, \gamma = 10$ for both $d = 1, 2$ cases. In addition, we set $N_r = 8 \times 10^3, 6 \times 10^4, N_a = N_b = 4 \times 10^2, 4 \times 10^4$, and $\alpha = 0.2, 0.5$ for $d = 1, 2$ respectively. Furthermore, we set $K_\varphi = 1, \tau_\eta = 0.02, \tau_\theta = 0.01, \gamma = 10$ for both $d = 3, 4$ cases, and set $K_u = 2, 4, N_r = 8 \times 10^4, 10^5, N_a = N_b = 7.5 \times 10^5, 1.28 \times 10^6, \alpha = 0.01, 0.0001$, and $\beta = 0.1, 0.001$ for $d = 3, 4$ respectively. Figure 11 shows the exact solution u^* (left) and the approximation u_θ (right) obtained by Algorithm 3 for dimension $d = 1$ case. In this case, $\Omega \times [0, T] = (-1, 1) \times [0, 1]$, and the horizontal axis is for t and vertical for x in Figure 11. After 10,000 iterations, the relative error $\|u_\theta - u^*\|_2 / \|u^*\|_2$ is 4.75%.

We also solve this problem for dimension $d = 2, 3, 4$, where the pointwise absolute errors (we take the $x_2 = \dots = x_d = 0$ slice for display when $d \geq 2$) are shown in Figure 12 (the horizontal axis is for t and vertical for x_1), and the total relative error versus the iteration number are shown in Figure 13. After 12,000 iterations, the relative errors are 2.13%, 3.12%, 1.20% for dimension $d = 2, 3, 4$, respectively.

5 Concluding Remarks

In this paper, we developed a transformative approach, called *weak adversarial network* or WAN, to solve general high-dimensional linear and nonlinear PDEs defined on arbitrary domains. Inspired by the weak formulation of PDEs, we rewrite the problem of finding the weak solution of the PDE as a saddle-point problem, where the weak solution and the test function are parameterized as the primal and adversarial networks, respectively. The objective function is completely determined by the PDE, the initial and boundary conditions, of the IBVP; and the parameters of these two networks are alternately updated during the training to reach optimum. The training only requires evaluations of the networks on randomly sampled collocations points in the interior and boundary of the domain, and hence can be completed quickly on desktop-level machines with standard deep learning configuration. We demonstrated the promising performance of WAN

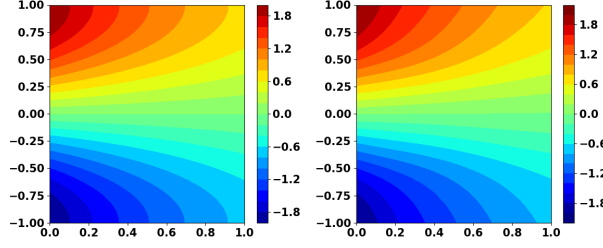


Figure 11: Exact solution u^* (left) and the approximation u_θ (right) obtained by Algorithm 3 for the diffusion-reaction equation (22) for $d = 1$ where $\Omega \times [0, T] = (-1, 1) \times [0, 1]$. Horizontal axis is for t and vertical for x .

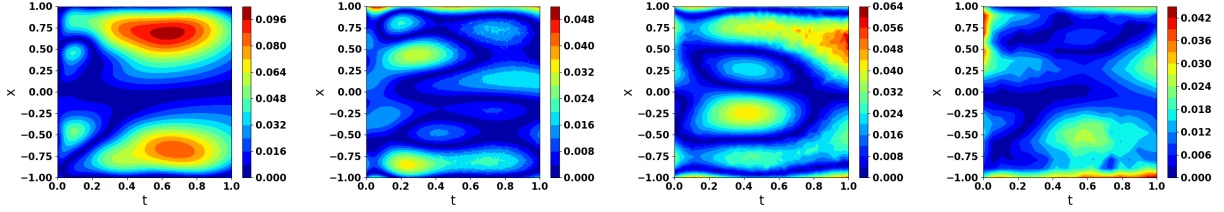


Figure 12: From left to right: pointwise absolute error $|u(x) - u^*(x)|$ obtained by Algorithm 3 after 12,000 iterations (10,000 for $d = 1$) on the diffusion-reaction equation (22) with $d = 1, 2, 3, 4$, respectively. For display purpose, the right three error images only show the slices of $x_2 = \dots = x_d = 0$ for $d \geq 2$ cases, respectively. Horizontal axis is for t and vertical for x_1 .

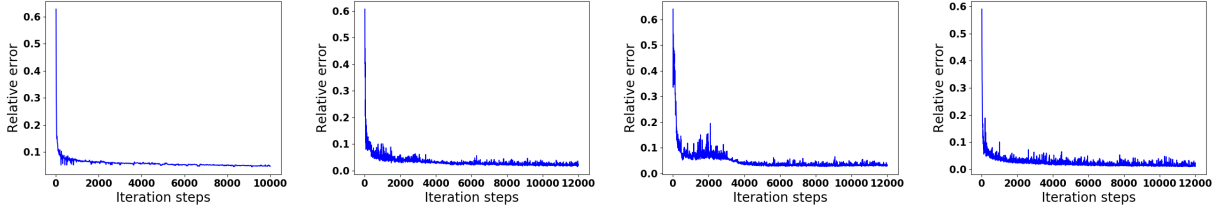


Figure 13: From left to right: relative errors versus iteration number of Algorithm 3 on the diffusion-reaction equation (22) for $d = 1, 2, 3, 4$, respectively.

on a variety of PDEs with high dimension, nonlinearity, and nonconvex domain which are challenging issues in classical numerical PDE methods. In all tests, WAN exhibits high efficiency and strong stability without suffering these issues.

References

- [1] W. F. Ames, Numerical methods for partial differential equations, Academic press, 2014.
- [2] K. Rudd, S. Ferrari, A constrained integration (cint) approach to solving partial differential equations using artificial neural networks, Neurocomputing 155 (2015) 277–285.
- [3] I. E. Lagaris, A. Likas, D. I. Fotiadis, Artificial neural networks for solving ordinary and partial differential equations, IEEE transactions on neural networks 9 (5) (1998) 987–1000.
- [4] M. Raissi, P. Perdikaris, G. Karniadakis, Physics-informed neural networks: A deep learning framework for solving forward and inverse problems involving nonlinear partial differential equations, Journal of Computational Physics 378 (2019) 686–707.
- [5] M. Raissi, P. Perdikaris, G. E. Karniadakis, Physics informed deep learning (part i): Data-driven solutions of nonlinear partial differential equations, arXiv preprint arXiv:1711.10561.

- [6] C. Beck, E. Weinan, A. Jentzen, Machine learning approximation algorithms for high-dimensional fully nonlinear partial differential equations and second-order backward stochastic differential equations, *Journal of Nonlinear Science* (2017) 1–57.
- [7] M. Fujii, A. Takahashi, M. Takahashi, Asymptotic expansion as prior knowledge in deep learning method for high dimensional bsdes, *Asia-Pacific Financial Markets* (2017) 1–18.
- [8] J. Han, A. Jentzen, E. Weinan, Overcoming the curse of dimensionality: Solving high-dimensional partial differential equations using deep learning, *arXiv preprint arXiv:1707.02568* (2017) 1–13.
- [9] E. Weinan, J. Han, A. Jentzen, Deep learning-based numerical methods for high-dimensional parabolic partial differential equations and backward stochastic differential equations, *Communications in Mathematics and Statistics* 5 (4) (2017) 349–380.
- [10] Y. Khoo, J. Lu, L. Ying, Solving for high-dimensional committor functions using artificial neural networks, *Research in the Mathematical Sciences* 6 (1) (2019) 1.
- [11] M. A. Nabian, H. Meidani, A deep neural network surrogate for high-dimensional random partial differential equations, *arXiv preprint arXiv:1806.02957*.
- [12] E. Weinan, B. Yu, The deep ritz method: A deep learning-based numerical algorithm for solving variational problems, *Communications in Mathematics and Statistics* 6 (1) (2018) 1–12.
- [13] A. Quarteroni, A. Valli, Numerical approximation of partial differential equations, Vol. 23, Springer Science & Business Media, 2008.
- [14] J. W. Thomas, Numerical partial differential equations: finite difference methods, Vol. 22, Springer Science & Business Media, 2013.
- [15] T. J. Hughes, The finite element method: linear static and dynamic finite element analysis, Courier Corporation, 2012.
- [16] H. Lee, I. S. Kang, Neural algorithm for solving differential equations, *Journal of Computational Physics* 91 (1) (1990) 110–131.
- [17] L. Wang, J. Mendel, Structured trainable networks for matrix algebra, in: 1990 IJCNN International Joint Conference on Neural Networks, IEEE, 1990, pp. 125–132.
- [18] D. Gobovic, M. E. Zaghloul, Analog cellular neural network with application to partial differential equations with variable mesh-size, in: Proceedings of IEEE International Symposium on Circuits and Systems-ISCAS'94, Vol. 6, IEEE, 1994, pp. 359–362.
- [19] R. Yentis, M. Zaghloul, Vlsi implementation of locally connected neural network for solving partial differential equations, *IEEE Transactions on Circuits and Systems I: Fundamental Theory and Applications* 43 (8) (1996) 687–690.
- [20] A. J. Meade Jr, A. A. Fernandez, The numerical solution of linear ordinary differential equations by feedforward neural networks, *Mathematical and Computer Modelling* 19 (12) (1994) 1–25.
- [21] A. J. Meade Jr, A. A. Fernandez, Solution of nonlinear ordinary differential equations by feedforward neural networks, *Mathematical and Computer Modelling* 20 (9) (1994) 19–44.
- [22] J. Tompson, K. Schlachter, P. Sprechmann, K. Perlin, Accelerating eulerian fluid simulation with convolutional networks, in: Proceedings of the 34th International Conference on Machine Learning-Volume 70, JMLR. org, 2017, pp. 3424–3433.
- [23] Y. Suzuki, Neural network-based discretization of nonlinear differential equations, *Neural Computing and Applications* (2017) 1–16.
- [24] J. Berg, K. Nyström, A unified deep artificial neural network approach to partial differential equations in complex geometries, *Neurocomputing* 317 (2018) 28–41.

- [25] M. Magill, F. Qureshi, H. de Haan, Neural networks trained to solve differential equations learn general representations, in: *Advances in Neural Information Processing Systems*, 2018, pp. 4071–4081.
- [26] M. Dissanayake, N. Phan-Thien, Neural-network-based approximations for solving partial differential equations, *communications in Numerical Methods in Engineering* 10 (3) (1994) 195–201.
- [27] J. Sirignano, K. Spiliopoulos, Dgm: A deep learning algorithm for solving partial differential equations, *Journal of Computational Physics* 375 (2018) 1339–1364.
- [28] D. Gilbarg, N. S. Trudinger, *Elliptic partial differential equations of second order*, springer, 2015.
- [29] J. Crank, P. Nicolson, A practical method for numerical evaluation of solutions of partial differential equations of the heat-conduction type, *Advances in Computational Mathematics* 6 (1) (1996) 207–226.
- [30] J. Duchi, E. Hazan, Y. Singer, Adaptive subgradient methods for online learning and stochastic optimization, *Journal of Machine Learning Research* 12 (Jul) (2011) 2121–2159.
- [31] M. Abadi, P. Barham, J. Chen, Z. Chen, A. Davis, J. Dean, M. Devin, S. Ghemawat, G. Irving, M. Isard, et al., Tensorflow: A system for large-scale machine learning, in: *12th {USENIX} Symposium on Operating Systems Design and Implementation ({OSDI} 16)*, 2016, pp. 265–283.
- [32] R. J. LeVeque, *Finite difference methods for ordinary and partial differential equations: steady-state and time-dependent problems*, Vol. 98, Siam, 2007.